EUROPEAN LABORATORY FOR PARTICLE PHYSICS

CERN-EP/99-091
7 July 1999

Search for pair-produced leptoquarks in e^+e^- interactions at $\sqrt{s} \simeq 183$ GeV

The OPAL Collaboration

Abstract

A search for pair-produced leptoquarks has been performed using a sample of e^+e^- collision events collected by the OPAL detector at LEP at e^+e^- centre-of-mass energies of about 183 GeV. The data sample corresponds to an integrated luminosity of 55.9 pb^{-1}. The leptoquarks were assumed to be produced via couplings to the photon and the Z^0 and then to decay within a single fermion generation. No evidence for contributions from leptoquark pair production processes was observed. Lower limits on scalar and vector leptoquark masses are obtained. The existing limits are improved in the region of large decay branching ratio to quark-neutrino.

to be submitted to
European Physical Journal C

The OPAL Collaboration

G. Abbiendi[2], K. Ackerstaff[8], G. Alexander[23], J. Allison[16], K.J. Anderson[9], S. Anderson[12], S. Arcelli[17], S. Asai[24], S.F. Ashby[1], D. Axen[29], G. Azuelos[18,a], A.H. Ball[8], E. Barberio[8], R.J. Barlow[16], J.R. Batley[5], S. Baumann[3], J. Bechtluft[14], T. Behnke[27], K.W. Bell[20], G. Bella[23], A. Bellerive[9], S. Bentvelsen[8], S. Bethke[14], S. Betts[15], O. Biebel[14], A. Biguzzi[5], I.J. Bloodworth[1], P. Bock[11], J. Böhme[14], O. Boeriu[10], D. Bonacorsi[2], M. Boutemeur[33], S. Braibant[8], P. Bright-Thomas[1], L. Brigliadori[2], R.M. Brown[20], H.J. Burckhart[8], P. Capiluppi[2], R.K. Carnegie[6], A.A. Carter[13], J.R. Carter[5], C.Y. Chang[17], D.G. Charlton[1,b], D. Chrisman[4], C. Ciocca[2], P.E.L. Clarke[15], E. Clay[15], I. Cohen[23], J.E. Conboy[15], O.C. Cooke[8], J. Couchman[15], C. Couyoumtzelis[13], R.L. Coxe[9], M. Cuffiani[2], S. Dado[22], G.M. Dallavalle[2], S. Dallison[16], R. Davis[30], S. De Jong[12], A. de Roeck[8], P. Dervan[15], K. Desch[27], B. Dienes[32,h], M.S. Dixit[7], M. Donkers[6], J. Dubbert[33], E. Duchovni[26], G. Duckeck[33], I.P. Duerdoth[16], P.G. Estabrooks[6], E. Etzion[23], F. Fabbri[2], A. Fanfani[2], M. Fanti[2], A.A. Faust[30], L. Feld[10], P. Ferrari[12], F. Fiedler[27], M. Fierro[2], I. Fleck[10], A. Frey[8], A. Fürtjes[8], D.I. Futyan[16], P. Gagnon[7], J.W. Gary[4], S.M. Gascon-Shotkin[17,i], G. Gaycken[27], C. Geich-Gimbel[3], G. Giacomelli[2], P. Giacomelli[2], W.R. Gibson[13], D.M. Gingrich[30,a], D. Glenzinski[9], J. Goldberg[22], W. Gorn[4], C. Grandi[2], K. Graham[28], E. Gross[26], J. Grunhaus[23], M. Gruwé[27], C. Hajdu[31] G.G. Hanson[12], M. Hansroul[8], M. Hapke[13], K. Harder[27], A. Harel[22], C.K. Hargrove[7], M. Harin-Dirac[4], M. Hauschild[8], C.M. Hawkes[1], R. Hawkings[27], R.J. Hemingway[6], G. Herten[10], R.D. Heuer[27], M.D. Hildreth[8], J.C. Hill[5], P.R. Hobson[25], A. Hocker[9], K. Hoffman[8], R.J. Homer[1], A.K. Honma[28,a], D. Horváth[31,c], K.R. Hossain[30], R. Howard[29], P. Hüntemeyer[27], P. Igo-Kemenes[11], D.C. Imrie[25], K. Ishii[24], F.R. Jacob[20], A. Jawahery[17], H. Jeremie[18], M. Jimack[1], C.R. Jones[5], P. Jovanovic[1], T.R. Junk[6], N. Kanaya[24], J. Kanzaki[24], D. Karlen[6], V. Kartvelishvili[16], K. Kawagoe[24], T. Kawamoto[24], P.I. Kayal[30], R.K. Keeler[28], R.G. Kellogg[17], B.W. Kennedy[20], D.H. Kim[19], A. Klier[26], T. Kobayashi[24], M. Kobel[3,d], T.P. Kokott[3], M. Kolrep[10], S. Komamiya[24], R.V. Kowalewski[28], T. Kress[4], P. Krieger[6], J. von Krogh[11], T. Kuhl[3], P. Kyberd[13], G.D. Lafferty[16], H. Landsman[22], D. Lanske[14], J. Lauber[15], I. Lawson[28], J.G. Layter[4], D. Lellouch[26], J. Letts[12], L. Levinson[26], R. Liebisch[11], J. Lillich[10], B. List[8], C. Littlewood[5], A.W. Lloyd[1], S.L. Lloyd[13], F.K. Loebinger[16], G.D. Long[28], M.J. Losty[7], J. Lu[29], J. Ludwig[10], D. Liu[12], A. Macchiolo[18], A. Macpherson[30], W. Mader[3], M. Mannelli[8], S. Marcellini[2], T.E. Marchant[16], A.J. Martin[13], J.P. Martin[18], G. Martinez[17], T. Mashimo[24], P. Mättig[26], W.J. McDonald[30], J. McKenna[29], E.A. Mckigney[15], T.J. McMahon[1], R.A. McPherson[28], F. Meijers[8], P. Mendez-Lorenzo[33], F.S. Merritt[9], H. Mes[7], I. Meyer[5], A. Michelini[2], S. Mihara[24], G. Mikenberg[26], D.J. Miller[15], W. Mohr[10], A. Montanari[2], T. Mori[24], K. Nagai[8], I. Nakamura[24], H.A. Neal[12,g], R. Nisius[8], S.W. O'Neale[1], F.G. Oakham[7], F. Odorici[2], H.O. Ogren[12], A. Okpara[11], M.J. Oreglia[9], S. Orito[24], G. Pásztor[31], J.R. Pater[16], G.N. Patrick[20], J. Patt[10], R. Perez-Ochoa[8], S. Petzold[27], P. Pfeifenschneider[14], J.E. Pilcher[9], J. Pinfold[30], D.E. Plane[8], P. Poffenberger[28], B. Poli[2], J. Polok[8], M. Przybycień[8,e], A. Quadt[8], C. Rembser[8], H. Rick[8], S. Robertson[28], S.A. Robins[22], N. Rodning[30], J.M. Roney[28], S. Rosati[3], K. Roscoe[16], A.M. Rossi[2], Y. Rozen[22], K. Runge[10], O. Runolfsson[8], D.R. Rust[12], K. Sachs[10], T. Saeki[24], O. Sahr[33], W.M. Sang[25], E.K.G. Sarkisyan[23], C. Sbarra[29], A.D. Schaile[33], O. Schaile[33], P. Scharff-Hansen[8], J. Schieck[11], S. Schmitt[11], A. Schöning[8], M. Schröder[8], M. Schumacher[3], C. Schwick[8], W.G. Scott[20], R. Seuster[14], T.G. Shears[8], B.C. Shen[4], C.H. Shepherd-Themistocleous[5], P. Sherwood[15], G.P. Siroli[2], A. Skuja[17], A.M. Smith[8], G.A. Snow[17], R. Sobie[28], S. Söldner-Rembold[10,f], S. Spagnolo[20], M. Sproston[20], A. Stahl[3],

K. Stephens[16], K. Stoll[10], D. Strom[19], R. Ströhmer[33], B. Surrow[8], S.D. Talbot[1], P. Taras[18], S. Tarem[22], R. Teuscher[9], M. Thiergen[10], J. Thomas[15], M.A. Thomson[8], E. Torrence[8], S. Towers[6], T. Trefzger[33], I. Trigger[18], Z. Trócsányi[32,h], E. Tsur[23], M.F. Turner-Watson[1], I. Ueda[24], R. Van Kooten[12], P. Vannerem[10], M. Verzocchi[8], H. Voss[3], F. Wäckerle[10], A. Wagner[27], D. Waller[6], C.P. Ward[5], D.R. Ward[5], P.M. Watkins[1], A.T. Watson[1], N.K. Watson[1], P.S. Wells[8], N. Wermes[3], D. Wetterling[11] J.S. White[6], G.W. Wilson[16], J.A. Wilson[1], T.R. Wyatt[16], S. Yamashita[24], V. Zacek[18], D. Zer-Zion[8]

[1]School of Physics and Astronomy, University of Birmingham, Birmingham B15 2TT, UK
[2]Dipartimento di Fisica dell' Università di Bologna and INFN, I-40126 Bologna, Italy
[3]Physikalisches Institut, Universität Bonn, D-53115 Bonn, Germany
[4]Department of Physics, University of California, Riverside CA 92521, USA
[5]Cavendish Laboratory, Cambridge CB3 0HE, UK
[6]Ottawa-Carleton Institute for Physics, Department of Physics, Carleton University, Ottawa, Ontario K1S 5B6, Canada
[7]Centre for Research in Particle Physics, Carleton University, Ottawa, Ontario K1S 5B6, Canada
[8]CERN, European Organisation for Particle Physics, CH-1211 Geneva 23, Switzerland
[9]Enrico Fermi Institute and Department of Physics, University of Chicago, Chicago IL 60637, USA
[10]Fakultät für Physik, Albert Ludwigs Universität, D-79104 Freiburg, Germany
[11]Physikalisches Institut, Universität Heidelberg, D-69120 Heidelberg, Germany
[12]Indiana University, Department of Physics, Swain Hall West 117, Bloomington IN 47405, USA
[13]Queen Mary and Westfield College, University of London, London E1 4NS, UK
[14]Technische Hochschule Aachen, III Physikalisches Institut, Sommerfeldstrasse 26-28, D-52056 Aachen, Germany
[15]University College London, London WC1E 6BT, UK
[16]Department of Physics, Schuster Laboratory, The University, Manchester M13 9PL, UK
[17]Department of Physics, University of Maryland, College Park, MD 20742, USA
[18]Laboratoire de Physique Nucléaire, Université de Montréal, Montréal, Quebec H3C 3J7, Canada
[19]University of Oregon, Department of Physics, Eugene OR 97403, USA
[20]CLRC Rutherford Appleton Laboratory, Chilton, Didcot, Oxfordshire OX11 0QX, UK
[22]Department of Physics, Technion-Israel Institute of Technology, Haifa 32000, Israel
[23]Department of Physics and Astronomy, Tel Aviv University, Tel Aviv 69978, Israel
[24]International Centre for Elementary Particle Physics and Department of Physics, University of Tokyo, Tokyo 113-0033, and Kobe University, Kobe 657-8501, Japan
[25]Institute of Physical and Environmental Sciences, Brunel University, Uxbridge, Middlesex UB8 3PH, UK
[26]Particle Physics Department, Weizmann Institute of Science, Rehovot 76100, Israel
[27]Universität Hamburg/DESY, II Institut für Experimental Physik, Notkestrasse 85, D-22607 Hamburg, Germany
[28]University of Victoria, Department of Physics, P O Box 3055, Victoria BC V8W 3P6, Canada
[29]University of British Columbia, Department of Physics, Vancouver BC V6T 1Z1, Canada
[30]University of Alberta, Department of Physics, Edmonton AB T6G 2J1, Canada

[31]Research Institute for Particle and Nuclear Physics, H-1525 Budapest, P O Box 49, Hungary
[32]Institute of Nuclear Research, H-4001 Debrecen, P O Box 51, Hungary
[33]Ludwigs-Maximilians-Universität München, Sektion Physik, Am Coulombwall 1, D-85748 Garching, Germany

[a] and at TRIUMF, Vancouver, Canada V6T 2A3
[b] and Royal Society University Research Fellow
[c] and Institute of Nuclear Research, Debrecen, Hungary
[d] on leave of absence from the University of Freiburg
[e] and University of Mining and Metallurgy, Cracow
[f] and Heisenberg Fellow
[g] now at Yale University, Dept of Physics, New Haven, USA
[h] and Department of Experimental Physics, Lajos Kossuth University, Debrecen, Hungary.
[i] now at Universitè de Lyon-I-Claude Bernard

1 Introduction

In the Standard Model (SM) quarks and leptons appear as formally independent components. However, they show an apparent symmetry with respect to the family and multiplet structure of the electroweak interactions. It seems therefore natural that some theories beyond the SM [1] predict the existence of new bosonic fields, called leptoquarks (LQs), mediating interactions between quarks and leptons. The interactions of LQs with the known particles are usually described by an effective Lagrangian that satisfies the requirement of baryon and lepton number conservation and respects the $SU(3)_C \otimes SU(2)_L \otimes U(1)_Y$ symmetry of the SM [2]. This results in nine scalar (S) and nine vector (V) leptoquarks, grouped into weak isospin triplets (S_1 and V_1), doublets ($S_{1/2}$, $\tilde{S}_{1/2}$, $V_{1/2}$ and $\tilde{V}_{1/2}$) and singlets (S_0, $\tilde{S}_0$, V_0 and $\tilde{V}_0$) [1]. They are shown in Tables 1 and 2. Under these assumptions, only the mass and the couplings to right-handed and/or left-handed fermions, denoted by λ_R and λ_L, remain as free parameters, since the couplings to the electroweak gauge bosons are completely determined by the electric charge and the third component of the weak isospin. Moreover, in order not to contradict the existing indirect constraints on the leptoquark masses and couplings coming from low energy data such as rare decays [2, 3], the requirement that a given LQ couples to just one family of fermions is imposed.

Several experimental results constrain the existence of leptoquarks. Searches for events with LQ single production, where a first generation LQ could be formed as a resonance between an electron and a quark, were performed by the ZEUS and H1 experiments at the ep collider HERA [4] and by the LEP experiments [5]. In e^+e^- collisions the quark comes from a resolved photon emitted by one of the LEP beams. As the production process directly involves a LQ–lepton–quark interaction, limits on the LQ mass, M_{LQ}, can be derived as a function of the couplings, λ, to fermions. Leptoquark masses below about 80 GeV are excluded for λ values greater than a few 10^{-2} (about one order of magnitude smaller than the electromagnetic coupling $\lambda_e \simeq 0.3$). For $\lambda = \lambda_e$, H1 excludes LQ masses up to 275 GeV. Both LEP and FERMILAB experiments have searched for events with LQ pair production [6, 7], setting limits on M_{LQ} as a function of β, the branching ratio of decay into a charged lepton and a quark. On the contrary, these limits do not depend on the couplings to fermions because the LQ pair should be produced via coupling to the gauge bosons. First generation scalar LQs with masses lower than about 200 GeV are excluded, assuming $\beta \geq 0.5$, while for $\beta = 0$ the mass limit is 79 GeV (D0). Second generation LQs are excluded below 160 GeV, assuming $\beta = 0.5$, and below about 200 GeV, if $\beta = 1$. Third generation scalar leptoquarks with charge $|Q_{e.m.}| = \frac{2}{3}$ or $\frac{4}{3}$ and $\beta = 1$ are excluded for masses lower than 99 GeV by CDF, while D0 excludes third generation scalar leptoquarks with charge $|Q_{e.m.}| = \frac{1}{3}$ and $\beta = 0$ below masses of 94 GeV. In the same cases vector LQs belonging to the third generation are excluded for masses below 170 GeV (CDF) and 148 GeV (D0).

In principle, LQs of all three generations can be pair-produced in e^+e^- collisions at LEP, by s-channel γ or Z^0 exchange and, in the case of first generation LQs, by exchange of a quark in the t-channel [8]. Due to the existing upper limits on the couplings, λ, to fermions, the t-channel contribution to the first generation production cross-section is negligible so that, for a given LQ state [2], the cross-section depends on the mass, the electric charge and third com-

[1] In this paper the notation used in [3] is adopted. This is slightly different from the notation used in [2].

[2] In this paper "state" will be used to refer to a charge eigenstate within a multiplet. It will be denoted by

LQ	I_3	$Q_{e.m.}$	decay		coupling $\lambda_{L,R}$	β
S_0	0	$-1/3$	$e_L^- u_L$	:	λ_{LS_0}	$\frac{\lambda^2_{LS_0}+\lambda^2_{RS_0}}{2\lambda^2_{LS_0}+\lambda^2_{RS_0}}$
			$e_R^- u_R$	:	λ_{RS_0}	
			$\nu_e d_L$	:	$-\lambda_{LS_0}$	
$\tilde{S}_0$	0	$-4/3$	$e_R^- d_R$	:	$\lambda_{R\tilde{S}_0}$	1
S_1	1	2/3	$\nu_e u_L$	:	$\sqrt{2}\lambda_{LS_1}$	0
	0	$-1/3$	$\nu_e d_L$	:	$-\lambda_{LS_1}$	1/2
			$e_L^- u_L$	:	$-\lambda_{LS_1}$	
	-1	$-4/3$	$e_L^- d_L$	:	$-\sqrt{2}\lambda_{LS_1}$	1
$S_{1/2}$	1/2	$-2/3$	$\nu_e \overline{u}_L$	:	$\lambda_{LS_{1/2}}$	$\frac{\lambda^2_{RS_{1/2}}}{\lambda^2_{LS_{1/2}}+\lambda^2_{RS_{1/2}}}$
			$e_R^- \overline{d}_R$	:	$-\lambda_{RS_{1/2}}$	
	$-1/2$	$-5/3$	$e_L^- \overline{u}_L$	:	$\lambda_{LS_{1/2}}$	1
			$e_R^- \overline{u}_R$	:	$\lambda_{RS_{1/2}}$	
$\tilde{S}_{1/2}$	1/2	1/3	$\nu_e \overline{d}_L$	:	$\lambda_{L\tilde{S}_{1/2}}$	0
	$-1/2$	$-2/3$	$e_L^- \overline{d}_L$	:	$\lambda_{L\tilde{S}_{1/2}}$	1

Table 1: *Quantum numbers and couplings for scalar leptoquarks. $Q_{e.m.}$ is the electric charge in units of e, I_3 the third component of the weak isospin and β denotes the branching ratio of decay to a charged lepton and a quark. Under the assumption of coupling within a single generation the same table must be repeated for second and third generation with the obvious substitutions $e \to \mu, \tau$, $u \to c, t$ and $d \to s, b$.*

ponent of the weak isospin, but is independent of the λ couplings. On the other hand, for couplings smaller than $\mathcal{O}(10^{-5})$ the lifetime of leptoquarks would be sufficiently long to produce a secondary decay vertex, clearly detatched from the primary vertex, or even outside the detector. This topology is not considered here as the charged tracks are required to come from the interaction vertex. To summarize, the present analysis covers the region of values of the couplings to fermions from about 10^{-6} to 10^{-2}. The decay of a heavy LQ into a quark and

$S_I(Q_{e.m.})$ or $V_I(Q_{e.m.})$, where the index I represents the weak isospin while the number in parenthesis is the electric charge in units of e.

LQ	I_3	$Q_{e.m.}$	decay		coupling $\lambda_{L,R}$	β
V_0	0	$-2/3$	$e_L^- \overline{d}_R$	:	λ_{LV_0}	$\frac{\lambda^2_{LV_0}+\lambda^2_{RV_0}}{2\lambda^2_{LV_0}+\lambda^2_{RV_0}}$
			$e_R^- \overline{d}_L$	:	λ_{RV_0}	
			$\nu_e \overline{u}_R$	:	λ_{LV_0}	
$\tilde{V}_0$	0	$-5/3$	$e_R^- \overline{u}_L$	:	$\lambda_{R\tilde{V}_0}$	1
V_1	1	1/3	$\nu_e \overline{d}_R$	:	$\sqrt{2}\lambda_{LV_1}$	0
	0	$-2/3$	$\nu_e \overline{u}_R$	:	λ_{LV_1}	1/2
			$e_L^- \overline{d}_R$	:	$-\lambda_{LV_1}$	
	-1	$-5/3$	$e_L^- \overline{u}_R$	:	$\sqrt{2}\lambda_{LV_1}$	1
$V_{1/2}$	1/2	$-1/3$	$\nu_e d_R$	:	$\lambda_{LV_{1/2}}$	$\frac{\lambda^2_{RV_{1/2}}}{\lambda^2_{LV_{1/2}}+\lambda^2_{RV_{1/2}}}$
			$e_R^- u_L$	:	$\lambda_{RV_{1/2}}$	
	$-1/2$	$-4/3$	$e_L^- d_R$	:	$\lambda_{LV_{1/2}}$	1
			$e_R^- d_L$	:	$\lambda_{RV_{1/2}}$	
$\tilde{V}_{1/2}$	1/2	2/3	$\nu_e u_R$	:	$\lambda_{L\tilde{V}_{1/2}}$	0
	$-1/2$	$-1/3$	$e_L^- u_R$	:	$\lambda_{L\tilde{V}_{1/2}}$	1

Table 2: *Quantum numbers and couplings for vector leptoquarks. $Q_{e.m.}$ is the electric charge in units of e, I_3 the third component of the weak isospin and β denotes the branching ratio of decay to a charged lepton and a quark. Under the assumption of coupling within a single generation the same table must be repeated for second and third generation with the obvious substitutions $e \to \mu, \tau$, $u \to c, t$ and $d \to s, b$.*

a charged lepton leads to final states characterized by an isolated energetic charged lepton, while for decays into a quark and a neutrino, the final state will have large missing energy. Therefore the following topologies can be considered for events that result from the decay of a leptoquark-antileptoquark pair:

Class A: two hadronic jets and two neutrinos; it includes the final states $\nu_e\overline{\nu_e}u\overline{u}$, $\nu_e\overline{\nu_e}d\overline{d}$, $\nu_\mu\overline{\nu_\mu}c\overline{c}$, $\nu_\mu\overline{\nu_\mu}s\overline{s}$ and $\nu_\tau\overline{\nu_\tau}b\overline{b}$.

Class B: two hadronic jets, one neutrino and one charged lepton of the first ($\nu_e eud$) or second generation ($\nu_\mu \mu cs$). In the hypothesis that each LQ couples to just one family of fermions, the

topology including two jets, one neutrino and one τ lepton is not possible at LEP, since one of the two jets would have originated in a top-quark.
Class C: two hadronic jets and one pair of oppositely charged leptons of the first or second generation, for example $e^+e^-u\overline{u}$ and $\mu^+\mu^-c\overline{c}$ respectively.
Class D: two hadronic jets and one pair of oppositely charged τ leptons, $\tau^+\tau^-b\overline{b}$. This case is considered separately from Class C because of the different possible τ decays.

In this paper a search is presented for pair-produced scalar leptoquarks of all three generations performed with the OPAL detector. Additionally, at this time, it was extended to vector leptoquarks of the first and second generation. The pair production process gives the advantage, with respect to single production by electron-quark interactions, that all states can be produced, included LQs coupling exclusively to neutrinos. Therefore searches for this channel at LEP give the possibility to explore the region of large decay branching ratio into quark-neutrino, where the FERMILAB experiments have reduced sensitivity. Moreover this is the first search for pair produced vector LQs at LEP. The study is based on data recorded during the 1997 LEP run at centre-of-mass energies, $\sqrt{s}$, between 181 and 184 GeV, corresponding to an integrated luminosity of 55.9 pb^{-1}. The luminosity weighted average of $\sqrt{s}$ is 182.7 GeV. Limits are derived under the assumption that only one state contributes to the cross-section. In the case of the third generation, mass limits will be given for scalar LQs which decay into a b-quark and either a τ-lepton or a τ-neutrino.

2 The OPAL Detector

The OPAL detector is described in detail in Ref. [9]. It is a multi-purpose apparatus having nearly complete solid angle coverage [3]. The central detector consists of two layers of silicon micro-strip detectors [10] surrounding the beam-pipe and a system of tracking chambers inside a 0.435 T solenoidal magnetic field. This system consists of a high-precision drift chamber, a large-volume jet chamber and a set of z-chambers measuring the track coordinates along the beam direction. A lead-glass electromagnetic calorimeter is located outside the magnet coil and covers the full azimuthal range in the polar angle range of
$|\cos\theta| < 0.984$. It is divided into two regions: the barrel ($|\cos\theta| < 0.82$) and the endcaps ($|\cos\theta| > 0.81$). The magnet return yoke, divided into barrel and endcap sections along with pole tips, is instrumented for hadron calorimetry in the region $|\cos\theta| < 0.99$. Four layers of muon chambers cover the outside of the hadron calorimeter. Close to the beam axis the forward calorimeter and gamma catcher together with the silicon-tungsten luminometer [11] complete the geometrical acceptance down to 33 mrad from the beam direction.

[3] The right-handed coordinate system is defined so that z is the coordinate parallel to the e^+ and e^- beams, with positive direction along the e^- beam; r is the coordinate normal to the beam axis, ϕ is the azimuthal angle with respect to the positive direction of the x-axis (pointing towards the centre of LEP) and θ is the polar angle with respect to $+z$.

3 Monte Carlo simulations

Neglecting the t-channel contribution, the differential cross sections for the production of a pair of leptoquarks of mass $\mathrm{M_{LQ}}$ in e^+e^- collisions at a centre-of-mass energy $\sqrt{s}$ are [8]:

$$\frac{d\sigma_S}{d\cos\theta} = \frac{3\pi\alpha^2}{8s}\left(1 - 4\mathrm{M}^2_{\mathrm{LQ}}/s\right)^{\frac{3}{2}} sin^2\theta \sum_{a=L,R} |k_a(s)|^2 \quad (1)$$

$$\frac{d\sigma_V}{d\cos\theta} = \frac{3\pi\alpha^2}{8\mathrm{M}^2_{\mathrm{LQ}}}\left(1 - 4\mathrm{M}^2_{\mathrm{LQ}}/s\right)^{\frac{3}{2}}\left[1 + \frac{1 - 3\left(1 - 4\mathrm{M}^2_{\mathrm{LQ}}/s\right)}{4}\sin^2\theta\right]\sum_{a=L,R} |k_a(s)|^2 \quad (2)$$

for scalar and vector LQs respectively. α is the electromagnetic coupling and

$$k_a(s) = -Q_{e.m.} + Q^Z_a(\mathrm{e})\frac{s}{s - M^2_Z + iM_Z\Gamma_Z}Q^Z(\mathrm{LQ}) \quad (3)$$

where $Q_{e.m.}$ is the LQ electric charge, M_Z and Γ_Z are the mass and the width of the weak neutral current gauge boson, and the couplings are given by

$$\begin{aligned} Q^Z(\mathrm{LQ}) &= \frac{I_3 - Q_{e.m.}\sin^2\theta_W}{\cos\theta_W\sin\theta_W} \\ Q^Z_L(\mathrm{e}) &= \frac{-\frac{1}{2} + \sin^2\theta_W}{\cos\theta_W\sin\theta_W} \\ Q^Z_R(\mathrm{e}) &= \tan\theta_W \end{aligned} \quad (4)$$

In equations 4 I_3 is the third component of the LQ weak isospin and θ_W is the Weinberg angle.

The Monte Carlo generator LQ2 [12] was used to simulate leptoquark pair events. Initial state QED radiation was included. The leptoquarks are assumed to decay isotropically in their rest frame and the hadronization of the final state $\mathrm{q\overline{q}'}$ pair was performed by JETSET [13]. Samples of 1000 signal events corresponding to different values of the leptoquark mass, from $\mathrm{M_{LQ}} = 50$ GeV to $\mathrm{M_{LQ}} = 90$ GeV in steps of 5 GeV, were generated for all the different decay topologies. The full simulation of the response of the OPAL detector [14] was performed on the generated events. Since they carry colour, leptoquarks may hadronize before decaying, if the couplings to fermions are small. This possibility was taken into account by introducing a systematic error on the detection efficiencies which was evaluated by using Monte Carlo samples in which the leptoquarks hadronized before decaying.

All relevant Standard Model background processes were studied using Monte Carlo generators. Two-fermion events ($\mathrm{Z}^{0*}/\gamma^* \to \mathrm{f\bar{f}}(\gamma)$, f = q,$\tau$) were simulated with PYTHIA [13] and KORALZ [15]. The Monte Carlo programs HERWIG [16] and PHOJET [17] were used to generate two-photon hadronic events. Other processes with four fermions in the final state, including W pair production, were simulated with grc4f [18] and Vermaseren [19].

4 Analysis

Charged tracks used in the calculation of physical variables were required to have their origin close to the $\mathrm{e^+e^-}$ interaction point, to have at least 20 measured space points in the jet chamber and at least 50% of the hits geometrically expected. The minimum transverse momentum

of the track with respect to the beam direction had to be greater than 120 MeV. Electromagnetic clusters were required to have an energy of at least 100 MeV in the barrel and 250 MeV in the endcaps. Endcap clusters were also required to contain at least two adjacent lead glass blocks. Clusters in the hadron calorimeter were rejected if their energy was smaller than 0.6 GeV (2 GeV in the hadron poletips, i.e. for $|\cos\theta| > 0.91$). To avoid double counting, calculations of experimental quantities such as visible energy, transverse momentum, etc., were performed following the method explained in [20].

All the different topologies of signal events (classes **A** to **D**) are characterized by large charged multiplicities and large energy depositions due to the hadronization of the $q\overline{q'}$ pair. In this analysis no attempt was made to identify the flavour of the quarks. Electron and muon identification, required in the selection of events of classes **B** and **C**, was performed by making a logical "OR" of different standard algorithms [21]. The electron identification is based on the energy match between a track and the associated cluster in the electromagnetic calorimeter and uses a minimum of subdetectors in order to give high efficiency, while the muon identification requires a minimum number of associated hits in either the muon chambers or hadron calorimeter strips. The energy of identified electrons was taken from the energy of the electromagnetic calorimeter cluster associated to the identified electron track.

4.1 The *jet jet* $\boldsymbol{\nu}$ $\boldsymbol{\nu}$ channel (class A)

Signal events of class **A** are characterized by an acoplanar pair of hadronic jets and missing energy. A few preselection requirements were applied to the data. To reduce beam-wall and beam-gas interactions, the fraction of charged tracks that satisfied the quality criteria given above was required to be greater than 0.2. A similar requirement was applied to the non-associated electromagnetic clusters. Both the number of accepted charged tracks and the number of accepted non-associated electromagnetic clusters had to exceed four. Finally, the total visible energy, E_{vis}, was required to be greater than $0.25\sqrt{s}$ and smaller than $1.25\sqrt{s}$. After the preselection, the following cuts were applied to the data:

A1) The events contained no identified charged electron or muon of energy greater than $0.12\sqrt{s}$.

A2) A two-dimensional cut was made in the plane $(p_t^{miss}/\sqrt{s})$ vs. $|\cos(\theta_{miss})|$, where p_t^{miss} is the missing transverse momentum with respect to the z-axis and $\cos(\theta_{miss})$ the cosine of the angle between the missing momentum and the z-axis. The cut is shown in Figure 1.

A3) The events were reconstructed into two jets using the Durham algorithm [22]: the sum of the energies of the two jets, E_{jets}, had to be such that $0.25\sqrt{s} < E_{jets} < 0.75\sqrt{s}$.

A4) The jets were required to be acolinear by asking that $\cos(\theta_{jj}) > -0.1$, where θ_{jj} is the angle between the two jet directions.

Cuts A1 and A2 are useful, in particular, in rejecting two-photon events and greatly reducing $Z^{0*}/\gamma^* \to f\bar{f}(\gamma)$ background. Cuts A3 and A4 completely reject $Z^{0*}/\gamma^* \to f\bar{f}(\gamma)$ events, and reduce four-fermion background.

	Data	**Background**	4-fermions	$\gamma\gamma$	$Z^{0*}/\gamma^* \to f\bar{f}(\gamma)$	ϵ_S^A (%)	ϵ_V^A (%)
(A1)	16281	14913	685	9308	4920	90.0	88.4
(A2)	87	80.9	52.2	1.6	27.1	59.4	58.7
(A3)	53	46.8	42.1	0.9	3.8	58.5	56.9
(A4)	4	3.6	2.7	0.8	<0.1	41.7	39.8

Table 3: *The remaining numbers of events after each cut of selection A for various background processes are compared with the data. The background is normalised to an integrated luminosity of 55.9 pb^{-1}. The last two columns report the signal efficiencies, in percent, for events with M_{LQ} = 85 GeV, for scalar and vector LQs respectively.*

Table 3 shows the number of events after each cut, compared with the number of background events as predicted from Monte Carlo samples, and the efficiencies for signal events corresponding to M_{LQ} = 85 GeV. Four events in the data survive the selections, in good agreement with the number of expected background events from Standard Model processes, 3.57 ± 0.83 (*stat.*).

4.2 The *jet jet* $l^{\pm}$ ν channel (class B)

After the application of the same preselection cuts described in section 4.1, the selection of signal events of class **B** proceeded as follows:

B1) The event was required to contain at least one identified electron or muon with an energy of at least $0.1\sqrt{s}$.

B2) No charged tracks and at most one (no) electromagnetic cluster within a cone of half-aperture 15° around the most energetic electron (muon).

B3) The missing transverse momentum had to be greater than $0.09\sqrt{s}$.

B4) A 2-dimensional cut in the plane $M_{l\nu}$ vs. $\cos(\theta_{l\nu})$ was applied as shown in Figure 2, where $\theta_{l\nu}$ is the angle between the momentum vector of the most energetic lepton and the missing momentum vector, while $M_{l\nu}$ is their invariant mass.

B5) After having removed the most energetic lepton, the event was forced into two jets using the Durham algorithm. The sum of the energies of the two jets, E_{jets}, had to be such that $0.25\sqrt{s} < E_{jets} < 0.75\sqrt{s}$. Moreover, a 2-dimensional cut in the plane $\cos(\theta_{jj})$ vs. M_{jj} was applied as shown in Figure 3, where θ_{jj} is the angle between the two jet directions and M_{jj} is the invariant mass of the two-jet system.

Two-photon events contribute negligibly to the background after selection B3. Cuts B2 and B3 are particularly efficient in reducing $Z^{0*}/\gamma^* \to f\bar{f}(\gamma)$ events.

In Table 4 the numbers of events after each cut are shown, compared with the numbers of predicted background events and the efficiencies for signal events corresponding to M_{LQ} = 85 GeV. One event in the data is retained after the selection for the first generation and three events for the second generation, in good agreement with an expected background of 2.22 ± 0.21 (*stat.*) and 2.84 ± 0.18 (*stat.*) events, respectively.

	Data	**Background**	4-fermions	$\gamma\gamma$	$Z^{0*}/\gamma^* \to f\bar{f}(\gamma)$	ϵ_S^B (%)	ϵ_V^B (%)
(B1)	1110/304	1106/321	277/151	28.4/2.5	801/169	89.1/87.7	90.7/90.1
(B2)	196/109	179/101	128/99.6	20.8/0.	30.2/1.4	79.8/80.3	81.7/79.9
(B3)	108/95	98.4/85.9	94.6/85.5	0.8/0.	3.0/0.4	73.5/72.3	75.2/73.6
(B4)	23/29	19.4/20.7	17.1/20.3	0.8/0.	1.5/0.4	59.8/58.8	60.4/61.7
(B5)	1/3	2.2/2.9	2.0/2.6	0./0.	0.2/0.3	43.1/49.1	43.6/51.5

Table 4: *The remaining numbers of events after each cut of selection B for various background processes are compared with the data. The background is normalised to an integrated luminosity of 55.9 pb^{-1}. The last two columns report the signal efficiencies, in percent, for events with* M_{LQ} *= 85 GeV, for scalar and vector LQs respectively. When two numbers are separated by a slash, the first one refers to the first generation and the second one to the second generation.*

4.3 The *jet jet* l^+ l^- channel (class C)

Signal events of this type have small missing energy and are characterized by the presence of a pair of high energy charged leptons of the same generation that tend to be isolated. The same preselections as for classes **A** and **B** were applied. The following cuts were then applied to select events:

C1) The presence of at least one pair of oppositely-charged identified electrons or muons was required. The most energetic leptons of the same generation and opposite in charge will be called the "pair" in the following. The energy of the most energetic lepton of the pair had to exceed $0.15\sqrt{s}$, while an energy of at least $0.1\sqrt{s}$ was required for the other lepton. For the first generation, the distributions of the energy of the most energetic electron of the pair for data, expected background and signal events corresponding to M_{LQ} = 85 GeV, are shown in Figure 4.

C2) No charged tracks and at most one (no) electromagnetic cluster within a cone of half-aperture 15° around the most energetic electron (muon). The same requirements, but considering a cone of half-aperture 10°, were applied for the less energetic lepton of the pair.

C3) The two leptons of the pair were required to be acolinear: $\cos(\theta_{ll}) > -0.85$, where θ_{ll} is the angle between the two leptons.

	Data	**Background**	4-fermions	$\gamma\gamma$	$Z^{0*}/\gamma^* \to f\bar{f}(\gamma)$	ϵ_S^C (%)	ϵ_V^C (%)
(C1)	97/10	96.0/7.4	19.9/4.3	0.4/0.	75.7/3.1	80.7/80.3	79.0/77.4
(C2)	2/2	2.8/1.5	2.7/1.5	0.1/0.	<0.1/0.	67.2/69.2	67.4/67.3
(C3)	2/2	1.6/1.0	1.6/1.0	0./0.	<0.1/0.	63.7/65.7	63.7/63.9

Table 5: *The remaining numbers of events after each cut of selection C for various background processes are compared with the data. The background is normalised to an integrated luminosity of 55.9 pb^{-1}. The last two columns report the signal efficiencies, in percent, for events with* M_{LQ} *= 85 GeV, for scalar and vector LQs respectively. When two numbers are separated by a slash, the first one refers to the first generation and the second one to the second generation.*

Background from two-photon events is removed after selection C1. Cut C2 suppresses $Z^{0*}/\gamma^* \to f\bar{f}(\gamma)$ events. The lepton acolinearity requirement C3 is useful in further reducing four-fermion back-

ground.

The numbers of events after each cut, compared with the numbers of expected background events and the efficiencies for signal events corresponding to $M_{LQ} = 85$ GeV, are shown in Table 5. After all cuts two candidates survive the selection both for the first and the second generation; 1.63 ± 0.14 (*stat.*) background events for the first generation and 0.98 ± 0.15 (*stat.*) for the second generation are expected.

4.4 The *jet jet* $\tau^+ \tau^-$ channel (class D)

Signal events of this type are characterized by a pair of isolated τ-leptons and a pair of energetic hadronic jets. The background comes predominantly from $Z^{0*}/\gamma^* \to f\bar{f}(\gamma)$ and four-fermion processes. The selection begins with the identification of τ lepton candidates, which is identical to that in [23], using three specific algorithms to identify semileptonic and hadronic τ-lepton decays. On average, 2.3 τ candidates per signal event are thus identified. The original τ-lepton direction is approximated by that of the visible decay products. The following requirements are then imposed:

D1) Events are required to contain at least nine charged tracks, and must have at least two τ-lepton candidates, including at least one pair whose members each have electric charge $|q| = 1$ and whose charges sum to zero. Pairs not fulfilling these requirements are not considered further.

D2) Events must have no more than 20 GeV of energy deposited in the forward calorimeter, gamma-catcher, and silicon-tungsten luminometer; a missing momentum vector satisfying $|\cos\theta_{miss}| < 0.97$, a total vector transverse momentum of at least $0.02\sqrt{s}$, and a scalar sum of all track and cluster transverse momenta larger than 40 GeV.

D3) Events must contain at least three jets, including single electrons and muons from τ-lepton decay which are allowed to be recognised as low-multiplicity jets, reconstructed using the cone algorithm as in [23] and no energetic isolated photons. An energetic isolated photon is defined as an electromagnetic cluster with energy larger than 15 GeV and no track within a cone of 30° half-angle.

D4) Events must contain no track or cluster with energy exceeding $0.3\sqrt{s}$.

For events surviving these requirements, the tracks and clusters not belonging to the τ pair (henceforth referred to as the "rest of the event" or RoE), are then split into two jets using the Durham algorithm. Two pairing schemes between the two τ candidates and the jets are thus possible. The invariant masses $m_{\tau j}$ of the two resulting τ-jet systems within each pairing scheme are then calculated using only the τ-lepton and jet momentum directions and requiring energy and momentum conservation. The pairing scheme exhibiting the lesser difference between $m_{\tau j1}$ and $m_{\tau j2}$ is then chosen. Then, in order for a τ candidate pair to be considered further, the following requirements on $m_{\tau j1}$ and $m_{\tau j2}$ are imposed, consistent with the hypothesis of the decay of two heavy objects of identical mass:

D5) Both $m_{\tau j1}$ and $m_{\tau j2}$ must be at least 30 GeV.

D6) The difference in invariant masses must be no more than 30% of their sum.

The distribution of $|m_{\tau j1}-m_{\tau j2}|/|m_{\tau j1}+m_{\tau j2}|$ is shown in Fig. 5 (a) for the data, the background events, and for a signal sample with $M_{LQ} = 85$ GeV. The resolution on $m_{\tau j}$ is typically less than 7 GeV, except very close to the kinematic limit.

A likelihood method [25, 26] is then applied to those events satisfying the above requirements, in order to select a final τ candidate pair for each event from those surviving, and to suppress further the remaining background. In each such event, for each remaining τ candidate pair and its associated hadronic RoE, a joint discriminating variable, $\mathcal{L}$, is constructed using normalised reference distributions generated from Monte Carlo samples of signal and background events. The set of variables for the reference distributions includes some which characterize each of the two τ-lepton candidates individually, some which describe their behavior as a pair and some which characterize the RoE. For those variables describing the τ candidates individually, separate reference distributions are generated for leptonic (electron or muon), hadronic 1-prong and hadronic 3-prong τ candidates, in order to exploit the differences between the three categories. Distributions of some of these input variables as well as that of $\mathcal{L}$ are shown in Fig. 5 (b) to (d). The τ candidate pair having the highest value of $\mathcal{L}$ is chosen as the definitive pair for each event, and the following requirement is then made:

D7) $\mathcal{L} > 0.93$

Table 6 shows the numbers of observed and expected events after each requirement, along with the detection efficiency for a signal with $M_{LQ} = 85$ GeV. Two events survive the selection while the background, predominantly from four-fermion processes, is estimated to be 2.07 ± 0.15 (*stat.*) events.

	Data	**Background**	4-fermions	$\gamma\gamma$	$Z^{0*}/\gamma^* \to ff(\gamma)$	ϵ_S^D (%)
(D1)	1322	1070	150	791	129	59.4
(D2)	209	191	129	3.0	59.1	57.8
(D3)	198	181	127	2.9	51.1	57.5
(D4)	149	139	100	2.2	36.3	56.2
(D5)	51	55.5	47.5	0.	8.0	52.7
(D6)	41	44.8	38.1	0.	6.7	50.2
(D7)	2	2.1	2.1	0.	<0.02	32.6

Table 6: *The remaining numbers of events after each cut of selection D for various background processes are compared with the data. The background is normalised to an integrated luminosity of 55.9 pb^{-1}. The last column reports the signal efficiency, in percent, for events with $M_{LQ} = 85$ GeV for scalar LQs.*

5 Results

The detection efficiencies for the different topologies of signal events, as a function of the leptoquark mass M_{LQ}, are listed in Table 7.

The systematic uncertainties in the number of signal events for the following sources were evaluated (they are quoted as relative %):

- The errors due to signal Monte Carlo statistics and the interpolation errors at an arbitrary point of M_{LQ} were estimated to be 5–10%, depending on the signal topology.

M_{LQ} (GeV)		50	60	70	80	85	90
Signal topology	Generation						
Class A (scalar)	1,2,3	14.3	23.9	31.4	37.0	41.7	42.8
Class A (vector)	1,2	15.0	22.7	32.3	36.3	39.8	42.3
Class B (scalar)	1	14.1	25.5	30.9	40.0	42.4	45.2
Class B (scalar)	2	15.1	28.9	38.2	44.8	49.1	52.5
Class B (vector)	1	13.9	23.0	35.5	41.7	43.6	46.7
Class B (vector)	2	15.3	25.8	38.5	47.0	51.5	53.9
Class C (scalar)	1	36.2	45.5	56.6	59.3	63.7	64.5
Class C (scalar)	2	37.1	46.1	55.9	62.9	65.7	67.0
Class C (vector)	1	33.8	43.0	52.8	62.1	63.7	67.0
Class C (vector)	2	35.5	41.7	53.4	63.0	63.9	66.8
Class D (scalar)	3	22.3	27.4	29.6	32.0	32.6	32.8

Table 7: *The detection efficiencies for the various selections, in percent, as a function of the leptoquark mass, M_{LQ}.*

- The error associated with the electron and muon identification method was evaluated using mixed events constructed by overlaying $Z^{0*}/\gamma^* \to q\overline{q}$ events with single hemispheres of $Z^{0*}/\gamma^* \to l^+l^-$ ($l = e, \mu$) events at $\sqrt{s} \approx M_{Z^0}$ [27]. Such events are topologically and kinematically analogous to $q\bar{q}l\nu$ events at $\sqrt{s} \approx 183$ GeV. This error was found to be 3.2% for electrons and 2.5% for muons. The error for τ identification was evaluated to be 1.2% [26].

- The uncertainty introduced by the modelling of the variables used in the selections was estimated to contribute with 5–15%. This was evaluated by displacing the cut values by an amount corresponding to the difference between the mean values of the data and background distributions. The corresponding displacement in the detection efficiencies was taken as a systematic error. The contributions from each single cut were added in quadrature.

- The uncertainty in the flavour of the final state quarks contributes with less than 6% for class **A** and with less than 3% for class **C**. This was evaluated by comparing the efficiencies corresponding to all the different possible flavours in a given decay channel, characterized by the leptons in the final state (for example $e^+e^-u\overline{u}$ and $e^+e^-d\overline{d}$ for class **C**, first generation). The value of the efficiency was taken to be the mean value and the largest difference between the mean and the single contributions was taken as a systematic error. In the case of classes **B** and **D** the flavours of the two quarks are precisely determined by the hypothesis of coupling within a single generation and (for class **D**) the top-quark mass threshold and thus no error is assigned.

- The systematic error associated with the fragmentation of the leptoquark decay products was estimated to be about 10%. This was evaluated by comparing the signal efficiencies with the efficiencies obtained by applying the same selection cuts to signal events in which the two LQs fragment before they decay.

- The error on the integrated luminosity was 0.5%.

The errors were considered to be independent and added in quadrature. A total systematic error of 10–30% was estimated on the number of expected background events, from the following sources: Monte Carlo statistics (10–20%), modelling of cut variables (10–25%), lepton identification (1.2–3.2%) and integrated luminosity (0.5%).

No evidence of leptoquark production was observed in the data. Upper limits at 95% confidence level (C.L.) on the LQ pair production cross-section $\sigma(e^+e^- \to LQ\overline{LQ})$ were computed from the observed numbers of events, the signal detection efficiencies and the number of expected background events, using the procedure described in [28]. The uncertainties both on the efficiencies and on the background were incorporated in the upper limits by numerical integration, assuming Gaussian distributions, as suggested in [29]. To obtain the limit at a given point in the plane β vs M_{LQ}, the independent analyses, corresponding to different classes of events, were combined by considering the total number of expected signal events. For example, for the first and the second generation, this number is given by

$$N_{exp}^{tot} \;=\; \sigma \;\cdot\; \int \mathcal{L} \;\cdot\; \left[\beta^2\epsilon^C + 2\beta(1-\beta)\epsilon^B + (1-\beta)^2\epsilon^A\right] \tag{5}$$

where σ is the production cross-section, $\int \mathcal{L}$ is the integrated luminosity of the data and $\epsilon^{A,B,C}$ are the signal detection efficiencies for classes A, B and C respectively.

Regions of the plane β vs M_{LQ} excluded at the 95% C.L. were determined by comparing the upper limits on the production cross-sections with the total cross-sections computed by integration of Equations 1 and 2. In the case of the third generation, limits have been evaluated for scalar states which decay only either into a τ-lepton and a b-quark, or into a ν_τ and a b-quark. For the third generation state $S_{1/2}(-2/3)$ only $\beta = 1$ can be considered since below the top-quark threshold only the right-handed coupling is possible. Figures 6 (a),(b) and 7 (a) show the upper limits of the production cross-sections as functions of the LQ mass, for scalar LQs with $\beta = 0$ and $\beta = 1$. The limit on $\tilde{S}_{1/2}(1/3)$ is valid for all three generations but the same is not true for the limit on $S_1(2/3)$, since the third generation state, under the hypothesis of diagonal coupling, would decay to a top-quark and a ν_τ. Figures 8 (a),(b) and 9 (a) show the upper limits of the production cross-sections as functions of the LQ mass, for vector LQs with $\beta = 1$, $\beta = 0.5$ and $\beta = 0$ respectively. The regions excluded in the plane β vs M_{LQ} of the states $S_{1/2}(-2/3)$, $V_{1/2}(-1/3)$ and $V_0(-2/3)$, whose β can range from 0 to 1 (0.5 to 1 for V_0) according to the relative weights of the left and right λ couplings, are reported in Figures 7 (b) and 9 (b) for the first and the second generation. The mass limits obtained from the present analysis are summarized in Table 8. Because of their much smaller cross-sections this search is not sensitive to the production of the states $S_0(-1/3)$ and $S_1(-1/3)$, so previous OPAL limits are quoted.

6 Conclusions

A data sample collected with the OPAL detector at $\sqrt{s} = 183$ GeV, corresponding to an integrated luminosity of 55.9 pb^{-1}, was analysed to search for events with pair production of scalar and vector leptoquarks. The search included scalar states of all three generations and vector states of the first and second generation only. In the case of vector leptoquarks this is the first pair production search at LEP. The present analysis covers the region of small values

LQ	$Q_{e.m.}$	β	1^{st} gen.	2^{nd} gen.	3^{rd} gen.
S_0	$-1/3$	[0.5,1]	44.2(∗)	44.2(∗)	–
$\tilde{S}_0$	$-4/3$	1	85.8	85.5	82.7
$S_{1/2}$	$-2/3$	[0,1]	80.8(∗∗)	78.8(∗∗)	82.2(∗ ∗ ∗)
	$-5/3$	1	87.0	86.8	–
$\tilde{S}_{1/2}$	$+1/3$	0	71.6	71.6	71.6
	$-2/3$	1	81.8	81.5	76.9
S_1	$+2/3$	0	84.8	84.8	–
	$-1/3$	0.5	44.2(∗)	44.2(∗)	–
	$-4/3$	1	87.8	87.6	85.8
V_0	$-2/3$	[0.5,1]	85.8(∗∗)	85.1(∗∗)	–
$\tilde{V}_0$	$-5/3$	1	90.5	90.4	–
$V_{1/2}$	$-1/3$	[0,1]	88.0(∗∗)	87.5(∗∗)	–
	$-4/3$	1	90.1	90.0	–
$\tilde{V}_{1/2}$	$+2/3$	0	87.5	87.5	–
	$-1/3$	1	88.8	88.6	–
V_1	$+1/3$	0	89.8	89.8	–
	$-2/3$	0.5	85.8	85.1	–
	$-5/3$	1	90.8	90.7	–

Table 8: *Lower mass limits, in GeV, for scalar and vector leptoquarks as obtained from the present analysis.*
(∗) LEP1 limits from OPAL.
(∗∗) Minimum allowed value for M_{LQ}. See Figures 7(b) and 9(b) for limits as functions of β.
(∗ ∗ ∗) This limit is valid for $\beta = 1$ (i.e. $\lambda_L = 0$ below the top-quark threshold).

of the couplings, λ, to fermions (about from 10^{-6} to 10^{-2}). No significant excess with respect to Standard Model predictions was found in the data. Lower mass limits for leptoquarks were set, under the assumption that only one leptoquark contributes to the cross-section. The results improve previous LEP lower limits on scalar leptoquark masses by 25–40 GeV, depending on the leptoquark quantum numbers. With respect to the existing limits from CDF and D0 experiments, mass lower limits are improved by about 10 GeV, for first and second generation, in the region of small values of the branching ratio of decay to a charged lepton and a quark.

References

[1] J.C. Pati and A. Salam, Phys. Rev. **D10** (1974) 275;
E. Farhi and L. Susskind, Phys. Rep. **74** (1981) 277;
B. Schrempp and F. Schrempp, Phys. Lett. **B153** (1985) 101;
J.L. Hewett and T.G. Rizzo, Phys. Rep. **183** (1989) 193;
P.H. Frampton, Mod. Phys. Lett. **A7** (1992) 559;
J.L. Hewett and T.G. Rizzo, Phys. Rev. **D58** (1998).

[2] J. Buchmüller, R. Rückl and D. Wyler, Phys. Lett. **B191** (1987) 442.

[3] S. Davidson, D. Bailey and B.A. Campbell, Z. Phys. **C61** (1994) 613.

[4] ZEUS Collab., M. Derrick *et al.*, Phys. Lett. **B306** (1993) 173;
H1 Collab., T. Ahmed *et al.*, Z. Phys. **C64** (1994) 545;
H1 Collab., S. Aid *et al.*, Phys. Lett. **B369** (1996) 173.

[5] DELPHI Collab., P. Abreu *et al.*, Phys. Lett. **B446** (1999) 62.

[6] OPAL Collab., G. Alexander *et al.*, Phys. Lett. **B263** (1991) 123;
L3 Collab., B. Adeva *et al.*, Phys. Lett. **B261** (1991) 169;
DELPHI Collab., P. Abreu *et al.*, Phys. Lett. **B275** (1992) 222;
ALEPH Collab., D. Decamp *et al.*, Phys. Rep. **216** (1992) 253.

[7] CDF Collab., F. Abe *et al.*, Phys. Rev. Lett. **75** (1995) 1012;
CDF Collab., F. Abe *et al.*, Phys. Rev. Lett. **78** (1997) 2906;
CDF Collab., F. Abe *et al.*, Phys. Rev. Lett. **79** (1997) 4327;
CDF Collab., F. Abe *et al.*, Phys. Rev. Lett. **81** (1998) 4806;
D0 Collab., S. Abachi *et al.*, Phys. Rev. Lett. **75** (1995) 3618;
D0 Collab., S. Abachi *et al.*, Phys. Rev. Lett. **80** (1998) 2051;
D0 Collab., S. Abachi *et al.*, Phys. Rev. Lett. **81** (1998) 38.

[8] J. Blümlein and R. Rückl, Phys. Lett. **B304** (1993) 337;
J. Blümlein and E. Boos, Nucl. Phys. (Proc. Suppl.) **B37** (1994) 181.

[9] OPAL Collaboration, K. Ahmet et al., Nucl. Instr. and Meth. **A305** (1991) 275.

[10] S. Anderson *et al.*, Nucl. Instr. and Meth. **A403** (1998) 326.

[11] B.E. Anderson et al., IEEE Transactions on Nuclear Science **41** (1994) 845.

[12] D.M. Gingrich, in "Physics at LEP2", CERN 96-01,
eds. G. Altarelli, T. Sjöstrand and F. Zwirner, Vol. 2, 345.

[13] T. Sjöstrand, Comp. Phys. Comm. **39** (1986) 347;
T. Sjöstrand, PYTHIA 5.7 and JETSET7.4 Manual, CERN-TH 7112/93.

[14] J. Allison *et al.*, Nucl. Instr. and Meth. **A317** (1992) 47.

[15] S. Jadach, B.F.L. Ward and Z. Wąs, Comp. Phys. Comm. **79** (1994) 503.

[16] G. Marchesini, B.R. Webber, G. Abbiendi, I.G. Knowles, M.H. Seymour and L. Stanco,
Comp. Phys. Comm. **67** (1992) 465.

[17] R. Engel and J. Ranft, Phys. Rev. **D54** (1996) 4244;
R. Engel, Z. Phys. **C66** (1995) 203.

[18] J. Fujimoto *et al.*, KEK-CP-046 (1996).

[19] J.A.M. Vermaseren, Nucl. Phys. **B229** (1983) 347.

[20] OPAL Collab., K. Ackerstaff *et al.*, Phys. Lett. **B389** (1996) 616.

[21] OPAL Collab., K. Ackerstaff *et al.*, Phys. Lett. **B389** (1996) 416.

[22] S. Catani *et al.*, Phys. Lett. **B269** (1991) 432.

[23] OPAL Collab., K. Ackerstaff *et al.*, Eur. Phys. J. **C1** (1998) 425.

[24] OPAL Collab., K. Ackerstaff *et al.*, Eur. Phys. J. **C5** (1998) 19.

[25] OPAL Collab., G. Abbiendi *et al.*,
"Searches for R-Parity Violating Decays of Gauginos at 183 Gev at LEP",
CERN-EP/98-203, submitted to Eur. Phys. J. C.

[26] OPAL Collab., G. Abbiendi *et al.*,
"Search for R-Parity Violating Decays of Scalar Fermions at LEP",
CERN-EP/98-043, submitted to Eur. Phys. J. C.

[27] OPAL Collab., K. Ackerstaff *et al.*, Eur. Phys. J. **C1** (1998) 395.

[28] C. Caso *et al.*, (Particle Data Group), Eur. Phys. J. **C3** (1998) 1.

[29] R.D. Cousins and V.L. Highland, Nucl. Instr. and Meth. **A320** (1992) 331.

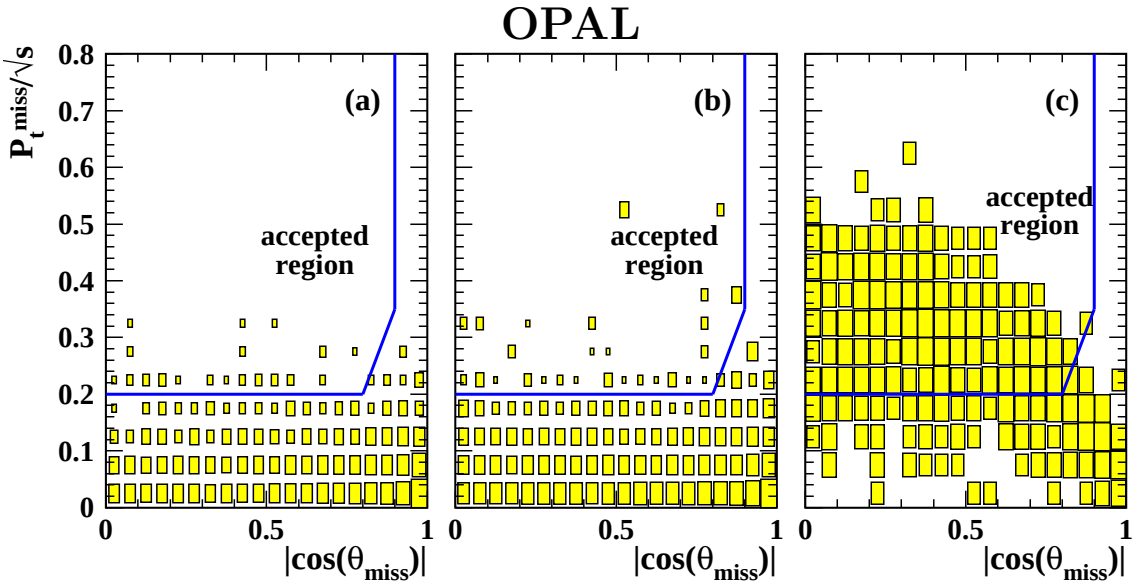

Figure 1:
Class **A**, the *jet jet* ν ν channel: The distribution of events in the plane $(p_t^{miss}/\sqrt{s})$ vs. $|\cos(\theta_{miss})|$, shown after the preselection and cut A1, for the data **(a)**, the simulated background **(b)** and simulated scalar LQ signal events of class **A** with M_{LQ} = 85 GeV **(c)**. The area of each box is proportional to the logarithm of the number of events falling within a two dimensional bin and is normalized with respect to the total content of each histogram separately.

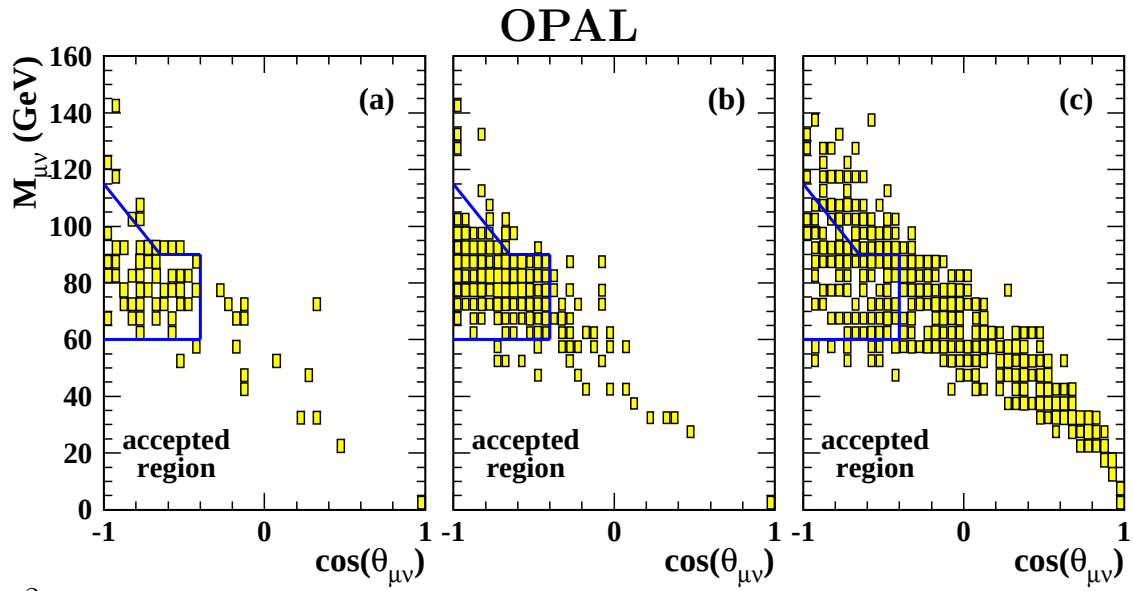

Figure 2:
Class **B**, the *jet jet l* ν channel: The distribution of events in the plane $M_{\mu\nu}$ vs. $\cos(\theta_{\mu\nu})$, shown after the preselection and cuts B1 – B3, for the data **(a)**, the simulated background **(b)** and simulated scalar LQ signal events of class B, second generation, with M_{LQ} = 85 GeV **(c)**. The area of each box is proportional to the logarithm of the number of events falling within a two dimensional bin and is normalized with respect to the total content of each histogram separately.

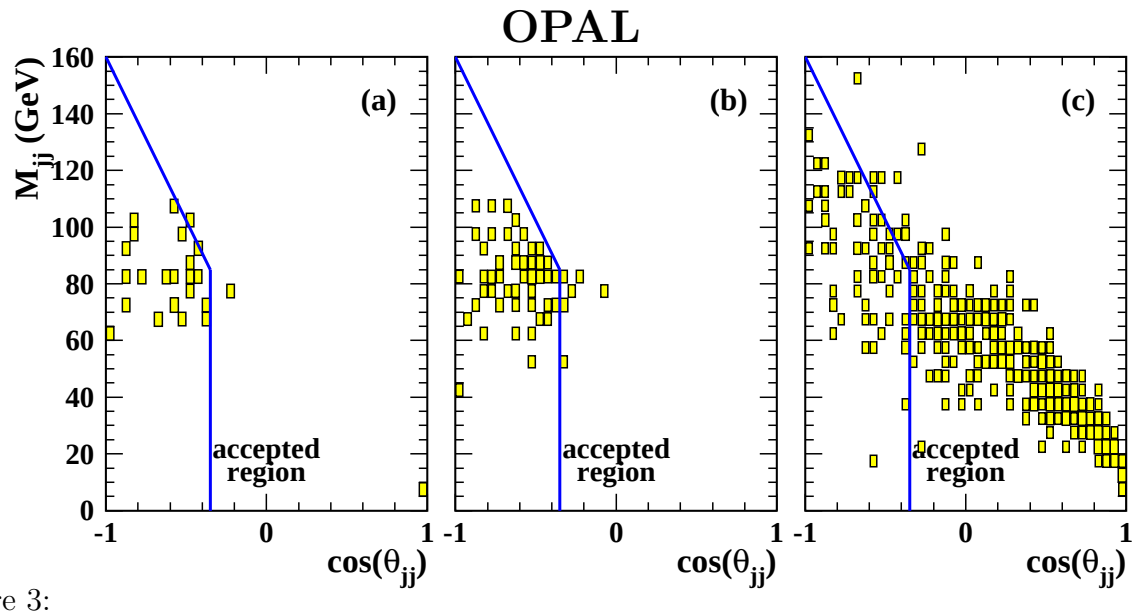

Figure 3:
Class **B**, the *jet jet l* ν channel: The distribution of events in the plane M_{jj} vs. $\cos(\theta_{jj})$, displayed after the preselection and cuts B1 – B4, for the data **(a)**, the total simulated background **(b)** and simulated scalar LQ signal events of class B with $M_{LQ} = 85$ GeV **(c)**. The area of each box is proportional to the logarithm of the number of events falling within a two dimensional bin and is normalized with respect to the total content of each histogram separately.

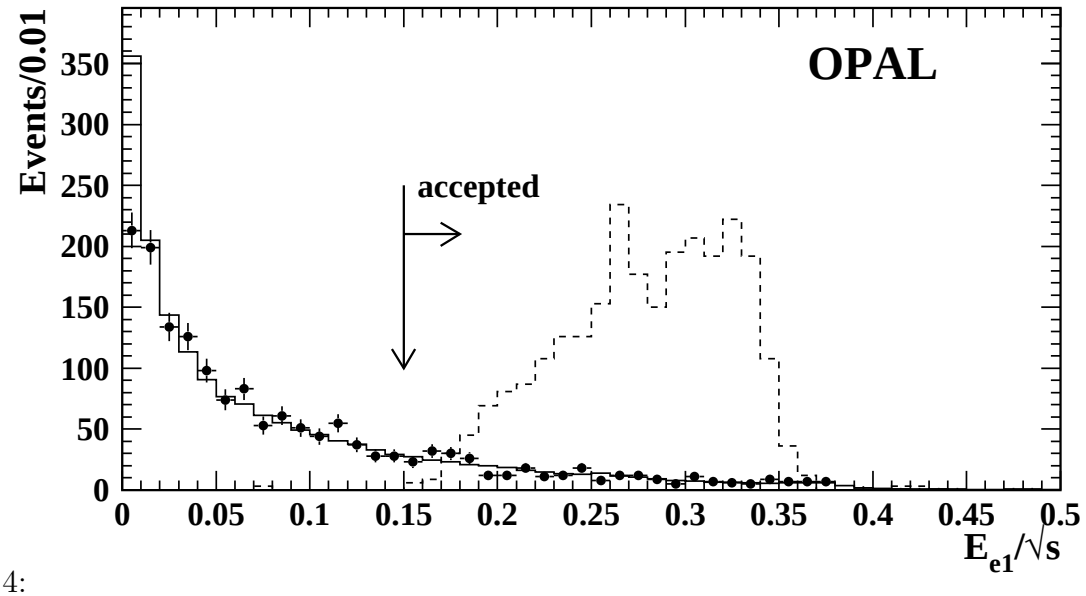

Figure 4:
Class **C**, the *jet jet* l^+ l^- channel: The distribution of the energy of the most energetic electron for events containing an electron pair after the preselections, for the data (points), the simulated background (full line, normalised to the integrated luminosity of the data) and a simulated signal (dashed line, arbitrary normalisation) corresponding to $M_{LQ} = 85$ GeV. The arrow denotes the position of cut C1.

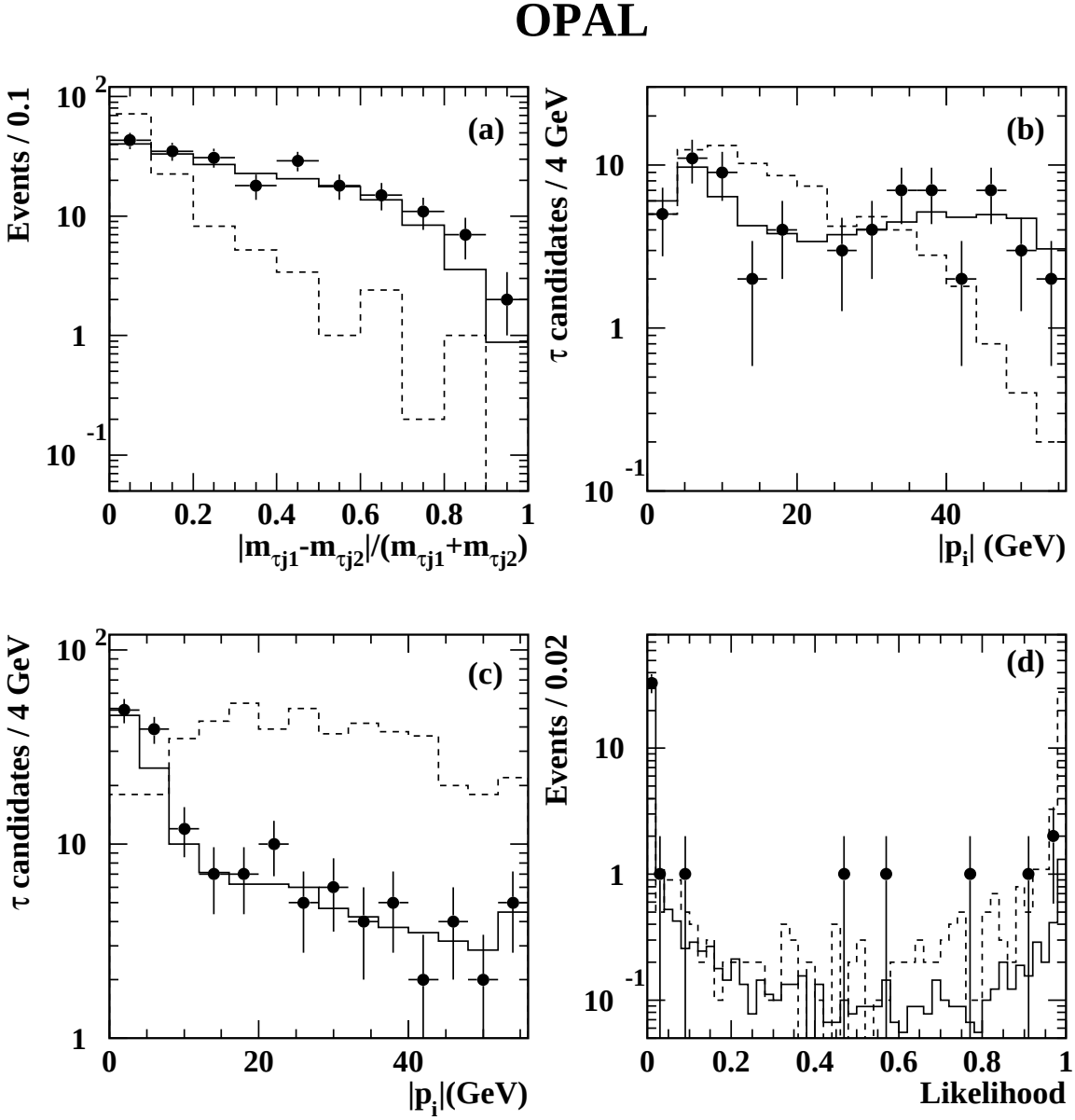

Figure 5:
Class **D**, the *jet jet* τ^+ τ^- channel: Kinematic distributions for the data (points), estimated Standard Model background (full line, normalised to the integrated luminosity of the data), and a simulated signal (dashed line, arbitrary normalisation) corresponding to $M_{LQ} = 85$ GeV. **(a)** Distribution of the difference in invariant mass of the tau-jet systems scaled by their sum after cut (D2).
Figures (b) and (c) demonstrate the difference in the distributions of the same likelihood input variable for two different categories of τ candidate, after cut (D4): **(b)** The momentum of leptonic τ candidates. **(c)** The momentum of 1-prong hadronic τ candidates. **(d)** The likelihood distribution after cut (D6).

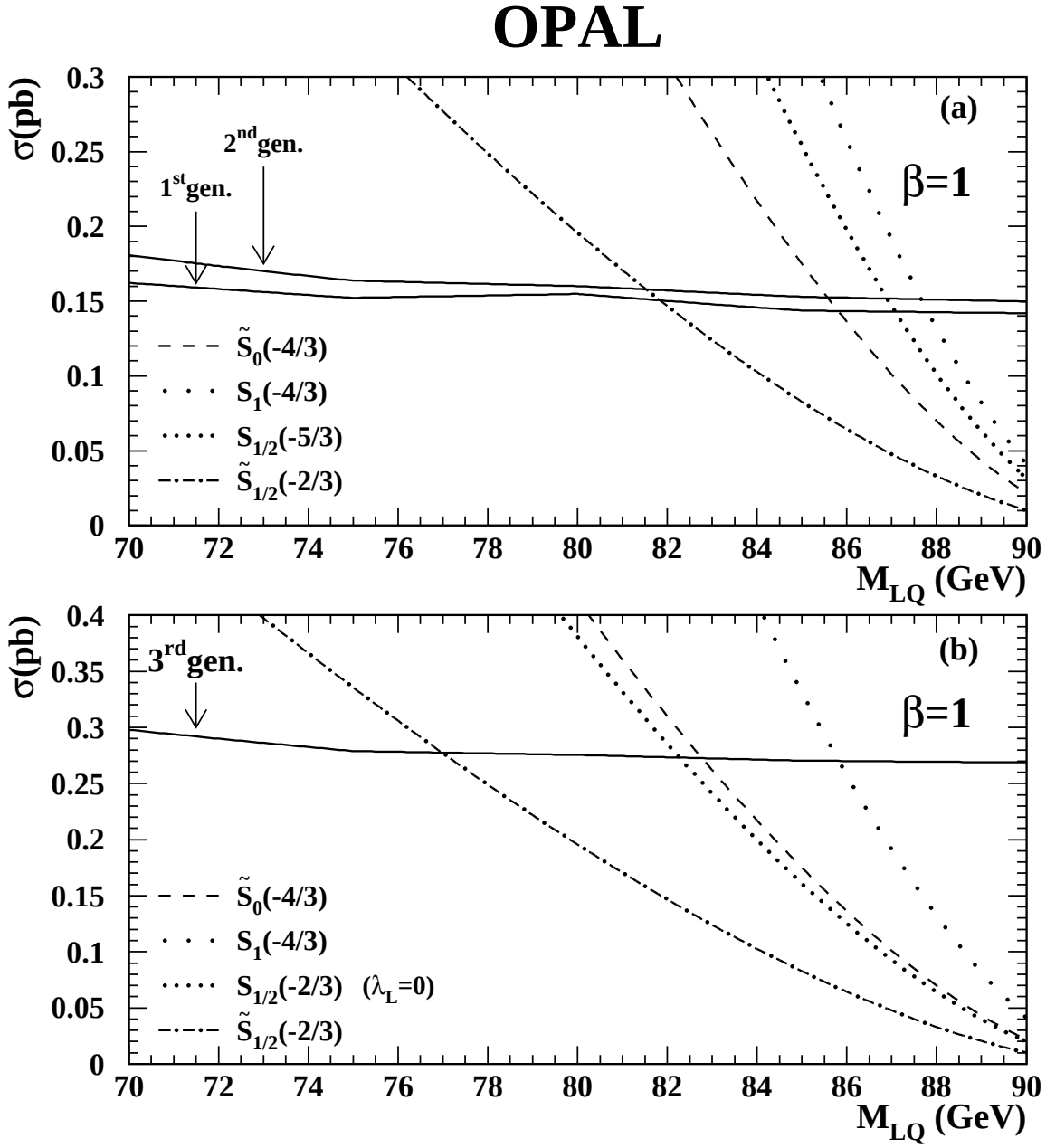

Figure 6:
(a) The 95% C.L. upper limits of the production cross-section for scalar LQs of the first and second generation with $\beta = 1$ (full lines) as a function of the LQ mass, compared with the theoretical production cross-sections. **(b)** Same as (a) for third generation scalar LQs.

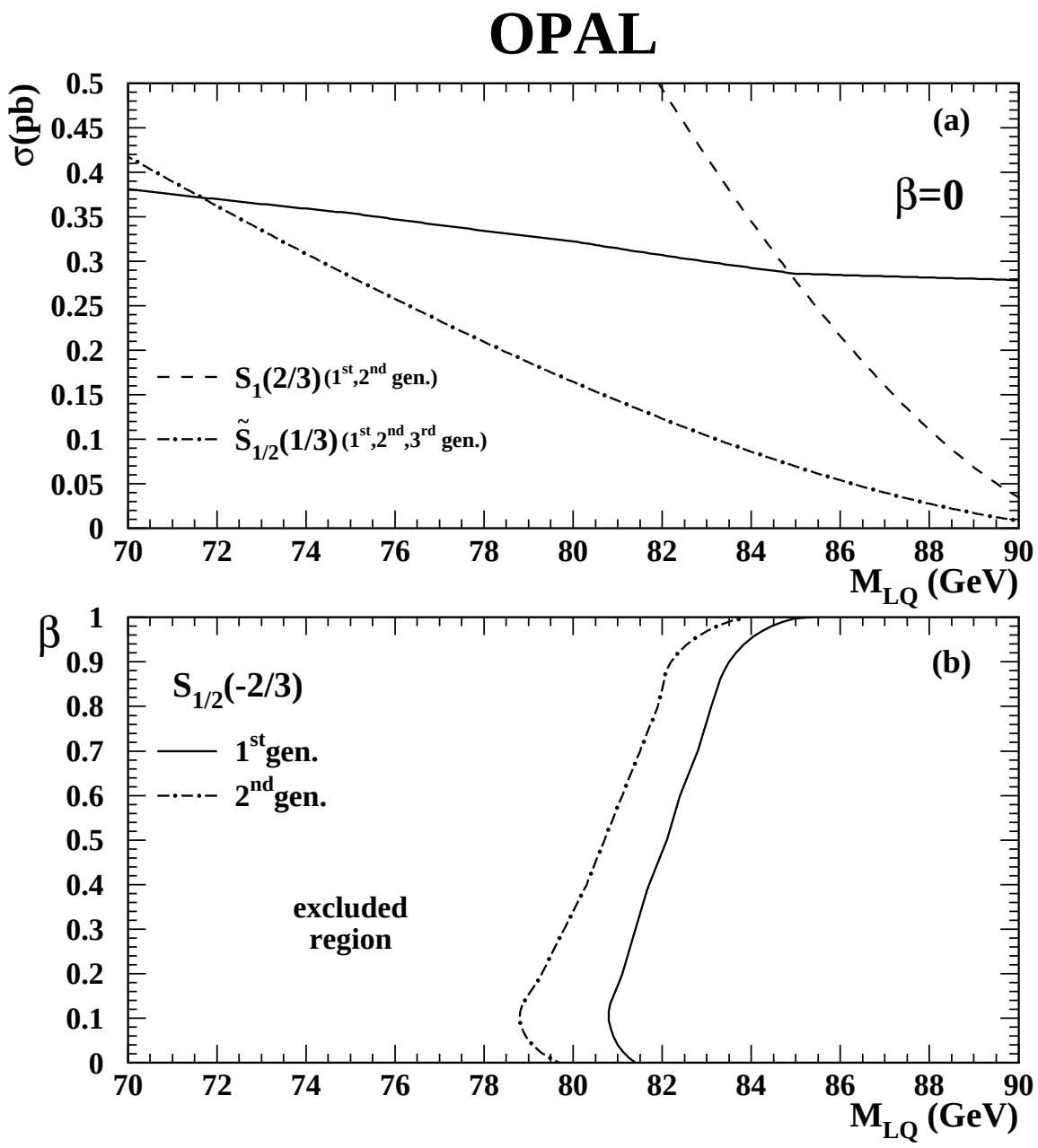

Figure 7:
(a) The 95% C.L. upper limit of the production cross-section for scalar LQs with $\beta = 0$ (full line) as a function of the LQ mass, compared with the theoretical production cross-sections. **(b)** The region of the plane β vs M_{LQ} excluded at the 95% C.L. for the state $S_{1/2}(-2/3)$ of the first and second generation.

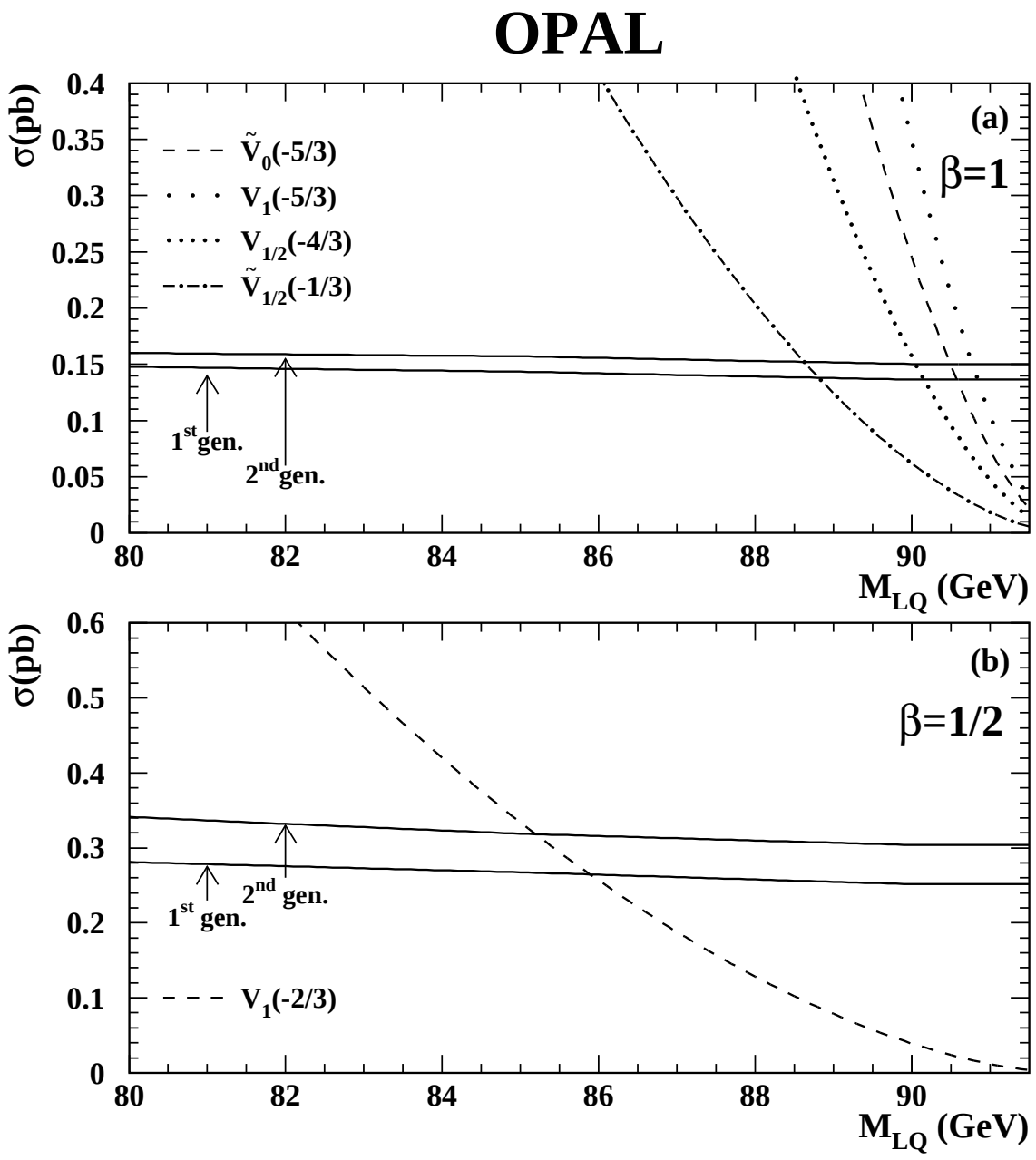

Figure 8:
(a) The 95% C.L. upper limits of the production cross-section for vector LQs of the first and second generation with $\beta = 1$ (full lines) as a function of the LQ mass, compared with the theoretical production cross-sections. **(b)** Same as (a) for vector LQs of the first and second generation with $\beta = 1/2$.

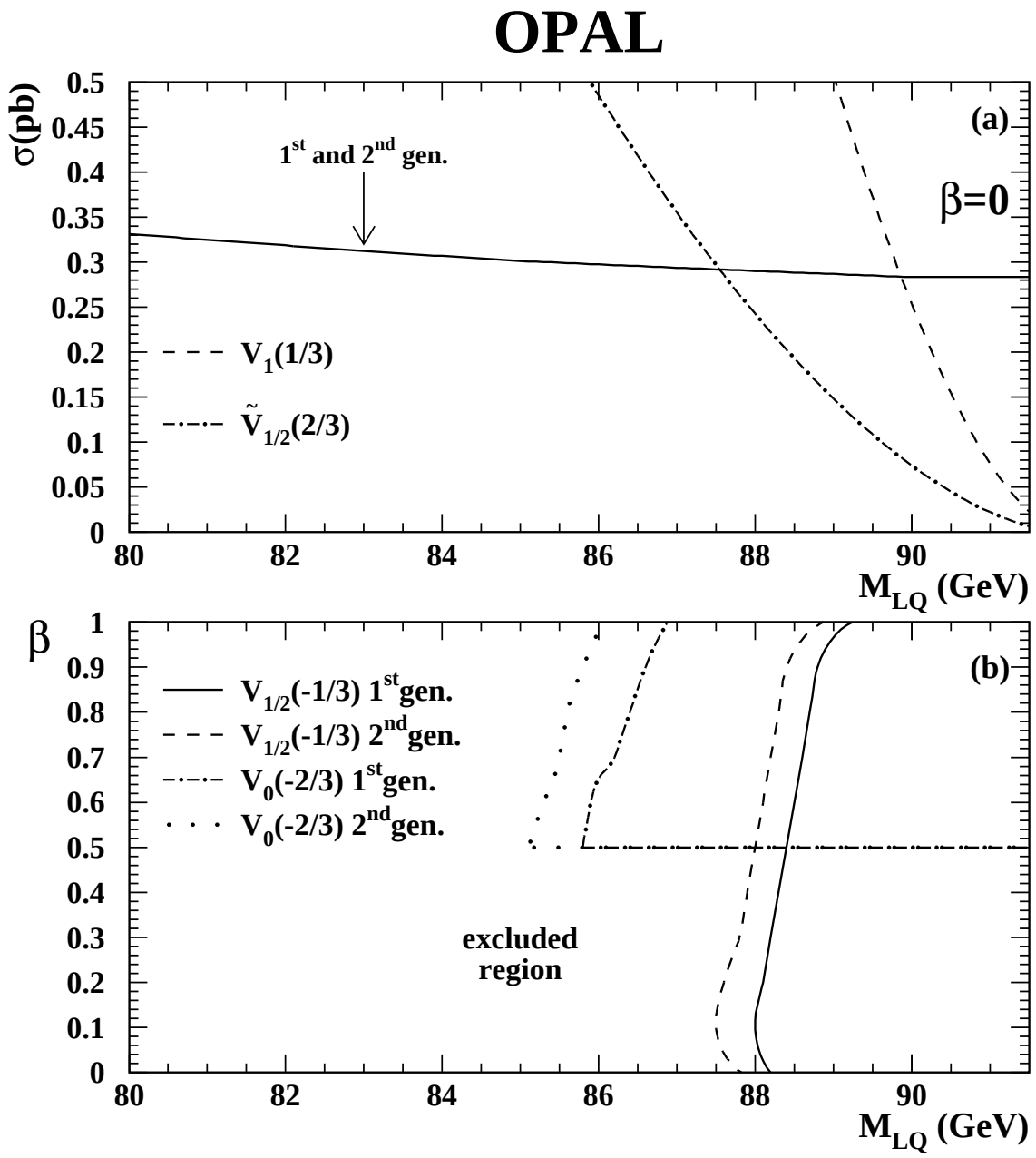

Figure 9:
(a) The 95% C.L. upper limit of the production cross-section for vector LQs with $\beta = 0$ (full line) as a function of the LQ mass, compared with the theoretical production cross-sections. **(b)** The region of the plane β vs M_{LQ} excluded at the 95% C.L. for the states $V_0(-2/3)$ and $V_{1/2}(-1/3)$ of the first and second generation.